JOURNAL OF PROPULSION AND POWER
Vol. 12, No. 6, November–December 1996

Triggering of Longitudinal Combustion Instabilities in Rocket Motors: Nonlinear Combustion Response

Josef M. Wicker,* William D. Greene,† Seung-Ill Kim,‡ and Vigor Yang§
Pennsylvania State University, University Park, Pennsylvania 16802

Pulsed oscillations in solid rocket motors are investigated with emphasis on nonlinear combustion response. The study employs a wave equation governing the unsteady motions in a two-phase flow, and a solution technique based on spatial and time averaging. A wide class of combustion response functions is studied to second order in fluctuation amplitude to determine if, when, and how triggered instabilities arise. Conditions for triggering are derived from analysis of limit cycles, and regions of triggering are found in parametric space. Based on the behavior of model dynamical systems, introduction of linear cross coupling and quadratic self-coupling among the acoustic modes appears to be the manner in which the nonlinear combustion response produces triggering to a stable limit cycle. Regions of initial conditions corresponding to stable pulses were found, suggesting that stability depends on initial phase angle and harmonic content, as well as the composite amplitude of the pulse.

Nomenclature

$\bar{a}$ = speed of sound in mixture
c_a, c_b = combustion response parameters, defined in Eqs. (45) and (56), respectively
EM = mechanical energy of acoustic wave
k_n = wave number of nth normal mode
L = combustion chamber length
M = Mach number
$\dot{m}_b$ = propellant burning rate
$\boldsymbol{n}$ = unit outward normal vector
p = pressure
r = amplitude of acoustic mode
$\boldsymbol{r}$ = spatial coordinates
R_c = combustion chamber radius
S = cross-sectional area
t = time
$\boldsymbol{u}$ = velocity vector
V = volume
α = linear growth constant
$\bar{\gamma}$ = mass-averaged specific heat ratio
η = time-varying amplitude of acoustic mode
Θ = phase-shift parameter, $-2\theta_1 + \theta_2$
θ = linear frequency shift
ρ = density
ϕ = phase angle of acoustic mode
Ψ = phase difference, $2\phi_1 - \phi_2$
ψ = normal mode shape
ω_n = radian frequency of nth normal mode

Superscripts
$'$ = fluctuation
$\bar{}$ = mean
$\cdot$ = time derivative

Received Sept. 28, 1995; revision received April 29, 1996; accepted for publication May 3, 1996.

*Graduate Student, Aerospace Engineering Department. Student Member AIAA.
†Graduate Student, Aerospace Engineering Department; currently at the NASA Marshall Space Flight Center, AL 35812.
‡Graduate Student, Mechanical Engineering Department; currently at Daewoo Motor Company, Republic of Korea.
§Professor, Mechanical Engineering Department. Associate Fellow AIAA.

I. Introduction

TRIGGERED combustion instability refers to initiation of unstable pressure oscillations by a finite amplitude pulse in a system that is otherwise stable to small perturbations. Although substantial effort has been expended in seeking the physical mechanisms involved in pulse-triggered instabilities and the analytical manifestations thereof, a comprehensive theory is currently unavailable. This work presents a model that is sufficient for producing simulated triggering phenomena in solid-propellant rocket motors. Owing to the analytical basis of this study, results obtained may be usefully applied to a general understanding of pulsed oscillations in other types of propulsion systems as well.

In a companion work to the present study, Yang et al.[1] established an approximate analysis based on the spatial and temporal averaging of the conservation equations to investigate the nonlinear behavior of unsteady motions in combustion chambers, with special attention focused on triggered combustion instabilities. Two important nonlinear processes, 1) pure acoustic coupling and 2) interactions between mean flow and nonlinear acoustics, were treated. The analysis indicated that pure acoustic nonlinearities do not lead to triggering of a finite disturbance to a limit cycle of any sort, even when third-order nonlinear acoustic motions were considered in the formulation. The coupling simply provides a mechanism for channeling energy among the acoustic modes. However, interactions between nonlinear acoustics and mean flow may cause an intrinsic modification of the stability characteristics of a system, depending on the ranges of linear parameters (i.e., growth constants and frequency shifts). The acoustic field may continuously extract energy from the mean flow and trigger a linearly stable system to execute an unstable limit cycle. Results did not show any conditions under which pulsing a linearly stable system would result in a stable limit cycle, a situation contrary to prior experience with both solid and liquid propellant rocket motors. Thus, to explain the observed phenomena of pulse-triggered combustion instability, mechanisms besides nonlinear gasdynamics must be investigated. The purpose of the present work is to study the influence of nonlinear combustion response[2,3] on the triggering of combustion instability. Various important aspects of triggered instability, including the functional form of combustion response with respect to acoustic oscillations and spectral content of the initial pulse, are investigated systematically.

The earliest theoretical study of triggering was initiated[4,5] in an effort to understand the dynamic stability behavior of liquid rocket engines. Combustion response was represented with a time-lag (i.e., n-τ) model, which did not yield triggering to a stable limit cycle. Based on the insight provided by Ref. 1 and the current study, it is now recognized that the type of mode coupling available through a simplified combustion scheme like the n-τ model is incapable of producing triggering. Although a linearly stable system may be pulsed to exhibit unstable limit cycle oscillations, such a model is incomplete since oscillations grow unbounded, and should not be considered as triggering in the actual sense.

Numerical investigations into triggered combustion instabilities have been conducted,[6-9] solving the complete conservation equations in one dimension. These studies successfully employed ad-hoc combustion response functions dependent on rectified velocity fluctuations to simulate observed characteristics of triggered oscillations. Similar analyses were used in a U.S. Air Force study on triggering in tactical motors,[10-12] and a multinational program on pulsed instability,[13,14] both of which had experimental emphasis. It is intended that the general conclusions generated from the current theoretical investigation may provide insight to supplement the detailed findings of the previous numerical and experimental studies.

In this work, the general two-phase formulation[15] is used to develop a nonlinear wave equation governing the behavior of chamber oscillations. Within this framework, multiple classes of nonlinear combustion response functions can be evaluated as mechanisms for sustaining triggered instability. By analyzing the dynamic behavior of the resulting systems, conditions required for triggering and requirements for stable initial pulses are investigated.

II. Formulation

Since combustion instability relies on the mutual coupling between acoustic waves and transient combustion response of a propellant, care must be taken in adequately representing the pertinent acoustic and combustion processes. The two-phase formulation of Culick and Yang[15] allows general treatment of the oscillatory flowfield and has shown much success in modeling unsteady behavior. The basic idea is to formulate governing equations for a single gas phase into which the effects of the condensed phase can be incorporated. The resulting expressions for conservation of mass, momentum, and energy may be written as

$$\frac{\partial \rho}{\partial t} + \boldsymbol{u}\cdot\nabla\rho = -\rho\nabla\cdot\boldsymbol{u} + W \tag{1}$$

$$\rho\frac{\partial \boldsymbol{u}}{\partial t} + \rho\boldsymbol{u}\cdot\nabla\boldsymbol{u} = -\nabla p + \boldsymbol{F} \tag{2}$$

$$\frac{\partial p}{\partial t} + \boldsymbol{u}\cdot\nabla p = -\bar{\gamma}p\nabla\cdot\boldsymbol{u} + P \tag{3}$$

The source terms W, $\boldsymbol{F}$, and P include the effects of viscosity, combustion, and interactions between the condensed and gas phases, and are defined in Ref. 15.

A perturbation expansion method is used to extract the behavior of unsteady motions in the system. The dependent variables are decomposed as sums of mean and fluctuating components:

$$\rho(\boldsymbol{r}, t) = \bar{\rho} + \rho'(\boldsymbol{r}, t), \qquad \boldsymbol{u}(\boldsymbol{r}, t) = \bar{\boldsymbol{u}}(\boldsymbol{r}) + \boldsymbol{u}'(\boldsymbol{r}, t)$$
$$p(\boldsymbol{r}, t) = \bar{p} + p'(\boldsymbol{r}, t), \ldots \tag{4}$$

The mean-flow Mach number is assumed to be small and of the same order of magnitude as the perturbation itself. Because spatial variations of mean density, pressure, and related thermodynamic properties are second-order in Mach number and appear as products with fluctuation quantities, they exert only third-order effects that may be neglected in this second-order analysis. Substituting the decomposed variables into Eqs. (1–3), using the ideal-gas equation of state, and rearranging the results yields a wave equation governing the oscillatory pressure field in the chamber:

$$\nabla^2 p' - \frac{1}{\bar{a}^2}\frac{\partial^2 p'}{\partial t^2} = h \tag{5}$$

The source term h represents the departure from classical acoustic solutions, and its exact definition depends on the order of analysis and the mechanisms under consideration. Boundary conditions on p' are specified in terms of the gradient of p' normal to the surface

$$\boldsymbol{n}\cdot\nabla p' = -f \tag{6}$$

In a solid rocket motor, treatment of this boundary condition is critical as the effect of unsteady combustion is exerted directly through the boundary along the burning surface. This point will be closely examined later.

To solve Eqs. (5) and (6), an approximate technique based on the Galerkin method[16,17] is employed. The fluctuating pressure and velocity fields are first expanded in terms of the acoustic normal modes ψ_n with time-varying coefficients:

$$p'(\boldsymbol{r}, t) = \bar{p}\sum_{n=1}^{\infty}\eta_n(t)\psi_n(\boldsymbol{r}) \tag{7}$$

$$\boldsymbol{u}'(\boldsymbol{r}, t) = \sum_{n=1}^{\infty}\frac{\dot{\eta}_n(t)}{\bar{\gamma}k_n^2}\nabla\psi_n(\boldsymbol{r}) \tag{8}$$

The normal-mode shapes satisfy the Helmholtz equation with homogeneous boundary conditions. Here $k_n = \omega_n/\bar{a}$ is the wave number. Because the magnitude of h is often on the order of the fluctuation amplitude, unsteady flowfields are correctly viewed as perturbations of classical acoustic motions; therefore, the series in Eqs. (7) and (8) should possess good convergence properties.

After spatially averaging Eq. (5) using the acoustic normal modes as weighting functions,[16] the following ordinary differential equations (ODEs) are derived for the behavior of pressure oscillations:

$$\frac{\mathrm{d}^2\eta_n}{\mathrm{d}t^2} + \omega_n^2\eta_n = F_n \tag{9}$$

where

$$F_n = -\frac{\bar{a}^2}{\bar{p}E_n^2}\left(\iiint h\psi_n\,\mathrm{d}V + \oiint f\psi_n\,\mathrm{d}S\right) \tag{10}$$

and E_n^2 is the Euclidean norm defined as

$$E_n^2 = \iiint \psi_n^2\,\mathrm{d}V \tag{11}$$

To second order in perturbation amplitude, the source terms h and f can be written as

$$h = -\nabla\cdot[\bar{\rho}(\bar{\boldsymbol{u}}\cdot\nabla\boldsymbol{u}' + \boldsymbol{u}'\cdot\nabla\bar{\boldsymbol{u}})] + \frac{1}{\bar{a}^2}\left(\bar{\gamma}\frac{\partial p'}{\partial t}\nabla\cdot\bar{\boldsymbol{u}} + \bar{\boldsymbol{u}}\cdot\nabla\frac{\partial p'}{\partial t}\right) - \nabla\cdot\left[\bar{\rho}(\boldsymbol{u}'\cdot\nabla\boldsymbol{u}') + \rho'\frac{\partial \boldsymbol{u}'}{\partial t}\right] + \frac{1}{\bar{a}^2}\left[\frac{\partial}{\partial t}(\boldsymbol{u}'\cdot\nabla p') + \bar{\gamma}\frac{\partial}{\partial t}(p'\nabla\cdot\boldsymbol{u}')\right] + \nabla\cdot\boldsymbol{F}' - \frac{1}{\bar{a}^2}\frac{\partial P'}{\partial t} \tag{12}$$

$$f = \left\{\left[\bar{\rho}\frac{\partial \boldsymbol{u}'}{\partial t} + \bar{\rho}(\bar{\boldsymbol{u}}\cdot\nabla\boldsymbol{u}' + \boldsymbol{u}'\cdot\nabla\bar{\boldsymbol{u}})\right] + \left[\rho'\frac{\partial \boldsymbol{u}'}{\partial t} + \bar{\rho}(\boldsymbol{u}'\cdot\nabla\boldsymbol{u}')\right] - \boldsymbol{F}'\right\}\cdot\boldsymbol{n} \tag{13}$$

where $\boldsymbol{F}'$ and P' represent the fluctuating influences of their respective source terms. Substitution into Eq. (10) yields an explicit expression for F_n, showing the basic physical processes that affect acoustic oscillations:

$$F_n = -\frac{\bar{a}^2}{E_n^2\bar{\rho}}\Bigg\{\underbrace{\bar{\rho}k_n^2\iiint \psi_n(\bar{\boldsymbol{u}}\cdot\boldsymbol{u}')\,dV}_{[a]} \underbrace{-\bar{\rho}\iiint[\boldsymbol{u}'\times(\nabla\times\bar{\boldsymbol{u}})]\cdot\nabla\psi_n\,dV}_{[b]} \underbrace{-\frac{1}{\bar{a}^2}\iiint\frac{\partial p'}{\partial t}\bar{\boldsymbol{u}}\cdot\nabla\psi_n\,dV}_{[c]}$$
$$\underbrace{+\frac{\bar{\gamma}-1}{\bar{a}^2}\iiint\psi_n\frac{\partial p'}{\partial t}\nabla\cdot\bar{\boldsymbol{u}}\,dV}_{[d]} \underbrace{+\bar{\rho}\iiint(\boldsymbol{u}'\cdot\nabla\boldsymbol{u}')\cdot\nabla\psi_n\,dV}_{[e]} \underbrace{-\frac{1}{\bar{a}^2}\iiint\frac{\partial p'}{\partial t}\boldsymbol{u}'\cdot\nabla\psi_n\,dV}_{[f]} \underbrace{+\frac{\bar{\gamma}-1}{\bar{a}^2}\iiint\psi_n\frac{\partial p'}{\partial t}\nabla\cdot\boldsymbol{u}'\,dV}_{[g]}$$
$$\underbrace{+\frac{\bar{\gamma}-1}{\bar{a}^2}\iiint\psi_n p'\nabla\cdot\frac{\partial \boldsymbol{u}'}{\partial t}\,dV}_{[h]} \underbrace{+\oiint\psi_n\frac{\partial}{\partial t}(\bar{\boldsymbol{u}}\rho' + \boldsymbol{u}'\bar{\rho} + \boldsymbol{u}'\rho')\cdot\boldsymbol{n}\,dS}_{[i]} \underbrace{-\iiint(\boldsymbol{F}'\cdot\nabla\psi_n) + \left(\frac{1}{\bar{a}^2}\psi_n\frac{\partial P'}{\partial t}\right)dV\Bigg\}}_{[j]} \tag{14}$$

The first four terms, [a]–[d] are referred to as the linear acoustics, and the next four terms, [e]–[h], are the second-order nonlinear acoustics. The last two terms, [i]–[j], are related to the boundary and volumetric effects, including combustion response.

By substituting Eqs. (7) and (8), F_n can be expressed in terms of the mode coefficients η_n. If specific attention is to be given certain physical processes (such as combustion response in the present work), the contributions to F_n may be conveniently separated:

$$F_n = (F_n)_L + (F_n)_{NG} + (F_n)_{NC} \tag{15}$$

The subscripts L, NG, and NC denote the effects of all linear mechanisms, nonlinear gasdynamics, and nonlinear combustion response, respectively. The form of $(F_n)_L$ and $(F_n)_{NG}$ in terms of η_n are as follows:

$$(F_n)_L = \sum_{i=1}^{\infty}(D_{ni}\dot{\eta}_i + E_{ni}\eta_i) \tag{16}$$

$$(F_n)_{NG} = -\sum_{i=1}^{\infty}\sum_{j=1}^{\infty}(A_{nij}\dot{\eta}_i\dot{\eta}_j + B_{nij}\eta_i\eta_j) \tag{17}$$

where the coefficients A_{nij}, B_{nij}, D_{ni}, and E_{ni} are defined in Refs. 2 and 3.

With F_n written in terms of η_n and $\dot{\eta}_n$, Eq. (9) can be solved using the time-averaging technique. The temporal evolution of unsteady motions in a rocket motor typically reveal two disparate time scales; the short time scale is proportional to ω_n^{-1}, measuring the rapid acoustic fluctuations, whereas gradual changes in amplitude and phase take place over the long time scale. Time-averaging filters rapid fluctuations from Eq. (9), leaving only the slowly varying characteristics of the oscillations. The resulting equations are not only easier to solve, but more importantly, allow clearer and deeper understanding of important nonlinear phenomena. The method proceeds by first transforming $\eta_n(t)$ to amplitude $r_n(t)$ and phase $\phi_n(t)$ as follows:

$$\eta_n(t) = r_n(t)\sin[\omega_n t + \phi_n(t)] \tag{18}$$

Equation (9) now becomes a set of first-order ODEs in r_n and ϕ_n, having rapidly and slowly varying sinusoidal terms. In time averaging the transformed equations over one period of the first mode, the slowly varying r_n and ϕ_n can be treated as constant. Because rapidly varying terms exert no net influence on the gradual behavior of each mode amplitude and phase, they disappear through the time averaging, resulting in the following equations:

$$\dot{r}_n = \alpha_n r_n - \frac{1}{4\omega_n}\sum_{i=1}^{\infty}\sum_{j=1}^{\infty} r_i r_j[(\omega_i\omega_j A_{nij} + B_{nij})\delta_{n,-i+j}\cos\phi_{n,i,-j} + (\omega_i\omega_j A_{nij} + B_{nij})\delta_{n,i-j}\cos\phi_{n,-i,j} + (\omega_i\omega_j A_{nij} - B_{nij})\delta_{n,i+j}\cos\phi_{n,-i,-j}] + (R_n)_{NC} \tag{19}$$

$$\dot{\phi}_n = -\theta_n + \frac{1}{4r_n\omega_n}\sum_{i=1}^{\infty}\sum_{j=1}^{\infty} r_i r_j[(\omega_i\omega_j A_{nij} + B_{nij})\delta_{n,-i+j}\sin\phi_{n,i,-j} + (\omega_i\omega_j A_{nij} + B_{nij})\delta_{n,i-j}\sin\phi_{n,-i,j} + (\omega_i\omega_j A_{nij} - B_{nij})\delta_{n,i+j}\sin\phi_{n,-i,-j}] + (\Phi_n)_{NC} \tag{20}$$

where

$$\phi_{n,\pm i,\pm j} = (\phi_n \pm \phi_i \pm \phi_j)$$

and $\delta_{n,k}$ is the Kronecker delta function. The coefficients α_n and θ_n are the linear growth constant and linear frequency shift, respectively, of the nth mode defined as

$$\alpha_n = -(D_{nn}/2) \qquad \theta_n = -(E_{nn}/2\omega_n)$$

In this article, all variables are nondimensionalized using L, $\bar{a}$, $L/\bar{a}$, and $\bar{\rho}$. The effects of nonlinear combustion response on the amplitude and phase are denoted by $(R_n)_{NC}$ and $(\Phi_n)_{NC}$, respectively, and the next section seeks explicit expressions for these terms.

III. Nonlinear Combustion Response

Combustion in solid motors takes place primarily in a thin layer near the propellant burning surface, and is most expeditiously treated as an effect of the boundary. Part [i] of Eq. (14) represents this influence as

$$\oiint\psi_n\frac{\partial}{\partial t}(\bar{\boldsymbol{u}}\rho' + \boldsymbol{u}'\bar{\rho} + \boldsymbol{u}'\rho')\cdot\boldsymbol{n}\,dS \tag{21}$$

where the integrand contains the unsteady part of mass flux normal to the boundary $\dot{m}_b'$.

$$\dot{m}_b' = -(\bar{\boldsymbol{u}}\rho' + \boldsymbol{u}'\bar{\rho} + \boldsymbol{u}'\rho')\cdot\boldsymbol{n} \tag{22}$$

Note that $\boldsymbol{n}$ is defined positive outward, and so a negative sign is added to the definition of $\dot{m}_b'$. Unfortunately, no comprehensive model for expressing the response of $\dot{m}_b'$ to acoustic motions exists, although this is a goal of ongoing research in combustion instability.[18–20] In this work, an ad-hoc combustion response function is used to specify $\dot{m}_b'$ in terms of physically viable dependences on acoustic fluctuations. The advantages of this method have been shown by Levine and Baum,[6,7] especially when qualitative results are sought over accurate quantitative details. Two general classes of ad-hoc functions will be examined, encompassing a broad range of pressure- and velocity-coupled combustion responses of practical interest.

A. Case I: $\dot{m}_b'$ Proportional to p'^2, u'^2, $p'u'$

In general, the unsteady burning rate of propellant depends on local pressure and velocity fluctuations, as combustion instabilities key on the interaction between acoustic oscillations and combustion processes. To second order in fluctuation magnitude, one sensible form would be quadratic response in p' and u', i.e., $\dot{m}_b'$ is proportional to any linear combination of the following quantities:

$$\dot{m}_b' \propto p'^2,\ u'^2,\ p'u' \tag{23}$$

Since the focus here is on nonlinear processes, linear response to p' and/or u' is contained in D_{ni} and E_{ni} through Eq. (16). Substituting Eqs. (7) and (8) into the most general form of the previous expression gives $(F_n)_{\mathrm{NC}}$ in terms of η_n:

$$(F_n)_{\mathrm{NC}} = \sum_{i=1}^{\infty}\sum_{j=1}^{\infty} P_{nij}\dot{\eta}_i\dot{\eta}_j + Q_{nij}\eta_i\eta_j + R_{nij}\dot{\eta}_i\eta_j \tag{24}$$

Here the coefficients P, Q, and R are constant values. By transforming Eq. (24) in terms of r_n and ϕ_n and time averaging the result, the nonlinear combustion-response forcing terms for the mode amplitudes and phases for case I become

$$\begin{aligned}(R_n)_{\mathrm{NC}} = \frac{1}{4\omega_n}\sum_{i=1}^{\infty}\sum_{j=1}^{\infty} r_i r_j[&(\omega_i\omega_j P_{nij} + Q_{nij})\delta_{n,-i+j}\cos\theta_{n,i,-j}\\ &+ (\omega_i\omega_j P_{nij} + Q_{nij})\delta_{n,i-j}\cos\theta_{n,-i,j}\\ &+ (\omega_i\omega_j P_{nij} - Q_{nij})\delta_{n,i+j}\cos\theta_{n,-i,-j}\\ &- \omega_i R_{nij}\delta_{n,-i+j}\sin\theta_{n,+i,-j} + \omega_i R_{nij}\delta_{n,i-j}\sin\theta_{n,-i,+j}\\ &- \omega_i R_{nij}\delta_{n,i+j}\sin\theta_{n,-i,-j}]\end{aligned} \tag{25}$$

$$\begin{aligned}(\Phi_n)_{\mathrm{NC}} = \frac{-1}{4r_n\omega_n}\sum_{i=1}^{\infty}\sum_{j=1}^{\infty} r_i r_j[&(\omega_i\omega_j P_{nij} + Q_{nij})\delta_{n,-i+j}\sin\phi_{n,i,-j}\\ &+ (\omega_i\omega_j P_{nij} + Q_{nij})\delta_{n,i-j}\sin\phi_{n,-i,j}\\ &+ (\omega_i\omega_j P_{nij} - Q_{nij})\delta_{n,i+j}\sin\phi_{n,-i,-j}\\ &+ \omega_i R_{nij}\delta_{n,-i+j}\cos\phi_{n,i,-j} - \omega_i R_{nij}\delta_{n,i-j}\cos\phi_{n,-i,j}\\ &+ \omega_i R_{nij}\delta_{n,i+j}\cos\phi_{n,-i,-j}]\end{aligned} \tag{26}$$

B. Case II: $\dot{m}_b'$ Proportional to $|u'|$, $|p'|$, $u'|p'|$, $p'|u'|$

Another physically reasonable set of nonlinear combustion responses involves the absolute value of oscillatory quantities. Specifically, the nonlinear combustion response may be proportional to any linear combination of the following quantities:

$$\dot{m}_b' \propto |u'|,\ |p'|,\ u'|p'|,\ p'|u'| \tag{27}$$

Of all the possible forms of this dependence, consideration of response only to $|u'|$ and $p'|u'|$ will suffice for the current study, as a simple phase shift can be used to translate from u' to p'. Furthermore, as will be shown later, these two cases embody two primary mechanisms for causing triggering. To help solidify the concepts behind the analysis, a brief justification of combustion response dependent upon $|u'|$ is desired.

Since heat release usually occurs in the close vicinity of the propellant surface, the coupling mechanisms involved in combustion response must take place near the boundary. For acoustic waves with fluctuating velocity vectors parallel to a solid surface, behavior near the surface is complicated by the no-slip condition that must be satisfied by the velocity field. In Refs. 18–20, both longitudinal and transverse velocity fluctuations are observed in this region, with varying amplitude and phase with respect to the acoustic wave. The penetration depth of the shear wave originating from the burning surface measures the thickness of this layer of multidimensional unsteadiness, which can be a significant fraction of chamber radius, depending primarily upon oscillation frequency and mean burning rate. The overall strength of the fluctuations is more or less proportional to the acoustic velocity in the core-flow region.

One theory explaining the effect of velocity fluctuations on propellant burning rate is that the unsteady motions augment the transfer of heat from the flame zone to the propellant, enhancing the transformation from solid phase to gaseous combustion products. Since the reaction zone thickness is much less than the penetration depth, combustion processes would experience any velocity oscillations within the unsteady layer. Such fluctuating vortical flowfields could indeed enhance convective heat transfer (to a degree proportional to the classical acoustic velocity). Crump and Price[21] claimed that turbulence associated with the unsteady velocity is responsible for the increase in heat transfer. Regardless of the exact details of the mechanism, compelling experimental evidence exists to justify the view that fluctuating velocity near the surface increases the burning rate. Notable are the findings of Ref. 21, in which the longitudinal profile of mean burning rate during a first mode longitudinal instability correlated very well with the acoustic velocity distribution along the longitudinal direction.

Typically, the structure of solid propellant grains has no preferred orientation with respect to combustion, and so only the magnitude of velocity in the combustion zone should be considered. In the works of Levine and Baum[6,7] and others, $|\bar{u} + u'|$ is identified as the quantity affecting velocity-coupled combustion response. For cases in which mean flow is greater than the amplitude of u', $\dot{m}_b'$ proportional to velocity magnitude would vary sinusoidally, giving a form of nonlinear combustion response similar to case I. However, the combustion zone occurs very close to the burning surface and the axial mean flow component is expected to be quite small there. Furthermore, if the two- and three-dimensional velocity fluctuations in the acoustic boundary layer are the cause of combustion enhancement, then mean flow might not be an important factor anyway. Thus, the response functions become for case IIa, $\dot{m}_b' \propto |u'|$:

$$\dot{m}_b'(t) = C_a|u'(t - \tau_n)| \tag{28}$$

and case IIb, $\dot{m}_b' \propto p'|u'|$:

$$\dot{m}_b'(t) = C_b p'(t - \tau_n)|u'(t - \tau_n)| \tag{29}$$

The τ_n allow for time lags in the response of combustion to the acoustic fluctuations; a different lag may be observed for each (nth) mode. Also, the coefficients C_a and C_b are dependent on frequency, in general, but are taken as constant here.

For longitudinal motions considered here, $|u'|$ may be expressed as

$$|u'| = \mathrm{sign}(u')\sum_{i=1}^{\infty}\frac{\dot{\eta}_i}{\bar{\gamma}k_i^2}\frac{\partial\psi_i}{\partial x} \tag{30}$$

For any number of longitudinal modes, sign(u') becomes

$$\text{sign}(u') = -\text{sign}(\dot{\eta}_1) \times \text{sign}\left[1 + \frac{\dot{\eta}_2}{2\dot{\eta}_1}\frac{\sin(k_2x)}{\sin(k_1x)} + \frac{\dot{\eta}_3}{3\dot{\eta}_1}\frac{\sin(k_3x)}{\sin(k_1x)} + \cdots\right] \quad (31)$$

Although the amplitude of the first mode is generally larger than the other modes, there may be times and locations where the term in brackets is negative. However, because the analysis is spatially and temporally averaged, it will suffice for our purposes to assume this term is always positive so that sign(u') = $-$sign($\dot{\eta}_1$). The resulting forcing, in terms of η_n, of the acoustic modes caused by nonlinear combustion response becomes the following:

Case IIa: $\dot{m}_b' \propto |u'|$:

$$(F_n)_{NC} = \frac{C_a}{\bar{\rho}E_n^2}\,\text{sign}[\dot{\eta}_1(t-\tau_1)]\sum_{i=1}^{\infty}\eta_i(t-\tau_i)I_{ni} \quad (32)$$

Case IIb: $\dot{m}_b' \propto p'|u'|$:

$$(F_n)_{NC} = \frac{C_b\bar{a}^2}{\bar{\gamma}E_n^2}\sum_{i=1}^{\infty}\sum_{j=1}^{\infty}\text{sign}[\dot{\eta}_1(t-\tau_1)] \times \left[\frac{\dot{\eta}_i(t-\tau_i)\dot{\eta}_j(t-\tau_j)}{k_j^2} - \eta_i(t-\tau_i)\eta_j(t-\tau_j)\right]K_{nij} \quad (33)$$

where

$$I_{ni} = \oiint \psi_n\frac{\partial\psi_i}{\partial x}\,dS, \qquad K_{nij} = \oiint \psi_n\psi_i\frac{\partial\psi_j}{\partial x}\,dS$$

The method of time averaging is applied to cases IIa and IIb in the same way as for case I, except that the integration over the fundamental period is partitioned to account for the changes of sign associated with $|u'|$. Expressions for $(R_n)_{NC}$ and $(\Phi_n)_{NC}$ become:

Case IIa:

$$(R_n)_{NC} = -\frac{C_a}{\pi\bar{\rho}E_n^2\omega_n}\sum_{i=1}^{\infty}r_iI_{ni}\left\{-\frac{1}{n+i}\cos[(n+i)\left(\frac{\pi}{2}-\phi\right) + (\phi_n+\phi_i) + \tau_1(\omega_n+\omega_i) - \omega_i\tau_i] + \frac{1}{n-i}\cos[(n-i)\left(\frac{\pi}{2}-\phi\right) + (\phi_n-\phi_i) + \tau_1(\omega_n-\omega_i) + \omega_i\tau_i]\right\} \quad (34)$$

$$(\Phi_n)_{NC} = \frac{C_a}{\pi\bar{\rho}E_n^2r_n\omega_n}\sum_{i=1}^{\infty}r_iI_{ni}\left\{-\frac{1}{n+i}\sin[(n+i)\left(\frac{\pi}{2}-\phi\right) + (\phi_n+\phi_i) + \tau_1(\omega_n+\omega_i) - \omega_i\tau_i] + \frac{1}{n-i}\sin[(n-i)\left(\frac{\pi}{2}-\phi\right) + (\phi_n-\phi_i) + \tau_1(\omega_n-\omega_i) + \omega_i\tau_i]\right\} \quad (35)$$

Case IIb:

$$(R_n)_{NC} = \frac{C_b\bar{a}^2}{2\pi\bar{\gamma}E_n^2\omega_n}\sum_{i=1}^{\infty}\sum_{j=1}^{\infty}r_ir_jK_{nij}[(\omega_i\omega_j/k_j^2+1) \times (G_{n+i+j}+G_{n-i-j}) + (\omega_i\omega_j/k_j^2-1)(G_{n+i-j}+G_{n-i+j})] \quad (36)$$

$$(\Phi_n)_{NC} = \frac{C_b\bar{a}^2}{2\pi\bar{\gamma}E_n^2r_n\omega_n}\sum_{i=1}^{\infty}\sum_{j=1}^{\infty}r_ir_jK_{nij}[(\omega_i\omega_j/k_j^2+1) \times (H_{n+i+j}+H_{n-i-j}) + (\omega_i\omega_j/k_j^2-1)(H_{n+i-j}+H_{n-i+j})] \quad (37)$$

where

$$G_{n\pm i\pm j} = \frac{1}{n\pm i\pm j}\sin\phi_{IIb}, \qquad H_{n\pm i\pm j} = -\frac{1}{n\pm i\pm j}\cos\phi_{IIb}$$

$$\phi_{IIb} = (n\pm i\pm j)(\pi/2-\phi_1) + \phi_n \pm \phi_i \pm \phi_j - (\pm\omega_i\tau_i \pm \omega_j\tau_j) + \tau_1(\omega_n \pm \omega_i \pm \omega_j)$$

IV. Analysis of Triggering Behavior

To maintain some degree of analytical tractability, only the first two longitudinal modes are retained in the expansions of acoustic pressure and velocity. These common modes adequately capture the major features of nonlinear behavior, since the amplitudes of higher modes are usually small because of the effective viscous damping at higher frequencies. Furthermore, Jahnke and Culick[22] suggest that while more modes indeed enhance accuracy, the essential physics of nonlinear intermodal energy transfer can be modeled by two modes, within certain limitations. Also, in their study of transverse mode instabilities, Yang and Culick[17] discovered that the form of mode coupling remains basically unchanged when going from a two-mode expansion to a three-mode expansion. Although actual combustors may have more modes in their spectra, the two-mode expansion captures the essential physics of the multiple degree of freedom, nonlinear system, with the first mode representative of low-frequency modes and the second representing higher frequency modes.

A. Case I: $\dot{m}_b'$ Proportional to p'^2, u'^2, $p'u'$

For nonlinear combustion response quadratic in pressure and velocity fluctuations, the governing equations for mode amplitude and phase become

$$\frac{dr_1}{dt} = \alpha_1r_1 - \beta r_1r_2\cos\Psi + \frac{r_1r_2}{4\omega_1}\{[(P_{112}+P_{121})\omega_1\omega_2 + Q_{112}+Q_{121}]\cos\Psi + (-R_{112}\omega_1 + R_{121}\omega_2)\sin\Psi\} \quad (38)$$

$$\frac{dr_2}{dt} = \alpha_2r_2 + \beta r_1^2\cos\Psi + \frac{r_1^2}{4\omega_2}[(P_{211}\omega_1^2 - Q_{211})\cos\Psi + R_{211}\omega_1\sin\Psi] \quad (39)$$

$$\frac{d\Psi}{dt} = \Theta + \left(2r_2 - \frac{r_1^2}{r_2}\right)\beta\sin\Psi - \frac{r_2}{2\omega_1}\{[(P_{112}+P_{121})\omega_1\omega_2 + Q_{112}+Q_{121}]\sin\Psi + (-R_{112}\omega_1 + R_{121}\omega_2)\cos\Psi\} + \frac{r_1^2}{4r_2\omega_2}[-(P_{211}\omega_1^2 - Q_{211})\sin\Psi + R_{211}\omega_1\cos\Psi] \quad (40)$$

where

$$\Psi = 2\phi_1 - \phi_2 \qquad \Theta = -2\theta_1 + \theta_2 \quad (41)$$

The two equations for the individual mode phases have been combined into one equation for Ψ, which is a measure of the phase difference between the two modes. The coefficient $\beta = (\bar{\gamma}+1)\omega_1/8\bar{\gamma}$ arises from nonlinear gasdynamic coupling. The coupling between the mode amplitudes is similar to that observed for second-order gasdynamics alone,[17] while the phase

angle difference plays a role similar to the case with mean flow-acoustic interactions.[1] Limit cycles appear as equilibrium points of Eqs. (38–40). It is found that for case I, a stable trivial solution ($\alpha_1 < 0$, $\alpha_2 < 0$) excludes a stable limit cycle; triggering to a stable limit cycle is impossible, although the system may trigger to an unstable limit cycle.

In a previous investigation of triggering (with focus on nonlinear gasdynamics), Yang et al.[1] analyzed the qualitative behavior of several classes of dynamical systems, with analogy drawn to nonlinear combustion instability. The conclusions from this portion of their study included the following:

1) Third-order nonlinearities are not necessary for triggering in multiple-degree-of-freedom systems.

2) In the multiple-degree-of-freedom models, quadratic self-coupling in one mode amplitude or linear cross coupling between the mode amplitudes was responsible for triggering to a stable limit cycle.

It is no surprise that case I does not exhibit triggering to a stable limit cycle, since neither quadratic self-coupling nor linear cross coupling are present. Therefore, the broad range of nonlinear pressure- and velocity-sensitive combustion response functions of case I will be excluded from the rest of this study as key mechanisms in causing triggered oscillations.

B. Case IIa: $\dot{m}_b'$ Proportional to $|u'|$

For $\dot{m}_b' \propto |u'|$, the amplitude and phase difference equations are

$$\frac{dr_1}{dt} = \alpha_1 r_1 - \beta r_1 r_2 \cos\Psi + 8c_a r_2 \left\{\frac{1}{3}\sin[\Psi + \omega_1(-3\tau_1 + 2\tau_2)] - \sin[\Psi + \omega_1(-\tau_1 + 2\tau_2)]\right\} \tag{42}$$

$$\frac{dr_2}{dt} = \alpha_2 r_2 + \beta r_1^2 \cos\Psi - c_a r_1 \left[\frac{4}{3}\sin(\Psi - 2\omega_1\tau_1)\right] \tag{43}$$

$$\frac{d\Psi}{dt} = \Theta + \left(2r_2 - \frac{r_1^2}{r_2}\right)\beta \sin\Psi - c_a\left(\frac{16r_2}{r_1}\left\{\frac{1}{3}\cos[\Psi + \omega_1(-3\tau_1 + 2\tau_2)] + \cos[\Psi + \omega_1(-\tau_1 + 2\tau_2)]\right\} + \frac{4r_1}{3r_2}\cos(\Psi - 2\omega_1\tau_1)\right) \tag{44}$$

where c_a is a parameter characterizing the nonlinear combustion response, defined as

$$c_a = \frac{C_a 8L}{\bar{\rho}\pi^2 3R_e} \tag{45}$$

and the parameters Θ, β, and α_n are defined as for case I.

To begin analysis of this system, the equilibrium states (limit cycles) are found as follows:

$$r_{10} = 0, \qquad r_{20} = 0 \quad \text{(trivial solution)} \tag{46}$$

$$r_{10} = (2\beta\cos\Psi_0)^{-1}(-3c_a\sin\Psi_0 \pm \sqrt{25c_a^2\sin^2\Psi_0 - 4\alpha_1\alpha_2}) \tag{47}$$

$$r_{20} = (c_a/\alpha_2)r_{10}\sin\Psi_0 - (\beta/\alpha_2)r_{10}^2\cos\Psi_0 \tag{48}$$

In these expressions and in the remaining analysis, zero time lag in the nonlinear combustion response has been used ($\tau_1 = \tau_2 = 0$). The phase difference for a limit cycle Ψ_0 may be found by setting Eq. (44) to zero and substituting the previous expressions. Only positive limit cycles are considered, since any case with negative amplitude is physically identical to one with positive amplitude, but with different phase. The conditions for a stable trivial solution become quite simple:

$$\alpha_1 < 0, \qquad \alpha_2 < 0, \qquad \alpha_1\alpha_2 > c_a^2\sin^2\Psi_{00} \tag{49}$$

where Ψ_{00} is the limiting value of phase difference for the trivial solution. The complicated expressions for stability of nonzero limit cycles lend themselves to numerical evaluation for assessment of triggering. Figure 1 shows the region on the α_1–α_2 parameter plane for which triggering is possible, given different combustion response parameters and $\Theta = 0.03$. For a fixed value of combustion response, there is a relatively small region of linear damping coefficients that will allow triggering. Triggering seems to require strong damping of the second mode and weak damping of the first. In actual systems that may have more than two modes, strong damping would be expected for one or more of the higher modes, with weak damping in lower mode(s). As combustion response becomes stronger, stronger linear damping of both modes is necessary to produce triggering. Also, Fig. 2 shows the region of triggering in the α_1–Θ plane for different values of combustion response and fixed second-mode growth rate. For the most part, a positive phase-shift parameter ($\Theta = -2\theta_1 + \theta_2$) is required to cause triggering to a stable limit cycle.

It is useful to consider the dynamics of the time-averaged mechanical energy EM_n of each mode. For longitudinal motion, the rates of change of EM_n become

$$\frac{dEM_1}{dt} = \frac{E_1^2}{\bar{\gamma}^2}(\alpha_1 r_1^2 - \beta r_1^2 r_2\cos\Psi - 4c_a r_1 r_2\sin\Psi) \tag{50}$$

$$\frac{dEM_2}{dt} = \frac{E_2^2}{\bar{\gamma}^2}(\alpha_2 r_2^2 + \beta r_1^2 r_2\cos\Psi - c_a r_1 r_2\sin\Psi) \tag{51}$$

The rate of change of energy within the entire system is simply the sum of the two previous expressions. Since α_1 and α_2 are always negative for triggering, the first terms in the previous equations represent energy dissipation by all linear processes, including viscous attenuation, linear combustion response, and particle damping, etc. The second terms are identified with the conservative energy transfer between the modes through nonlinear gasdynamics, and together they make no net contribution to total energy within the system. The remaining terms represent the rate at which energy is gained or lost in each mode because of the nonlinear combustion response, which can increase or decrease the energy in both modes depending on the value of $\sin\Psi$. Limit cycle oscillations are characterized by a balance of energy flow into and out of the modes. The transient behavior during which the oscillation damps out or seeks a limit cycle also is strongly influenced by the flow of energy within the system. In Refs. 10–12, it was concluded

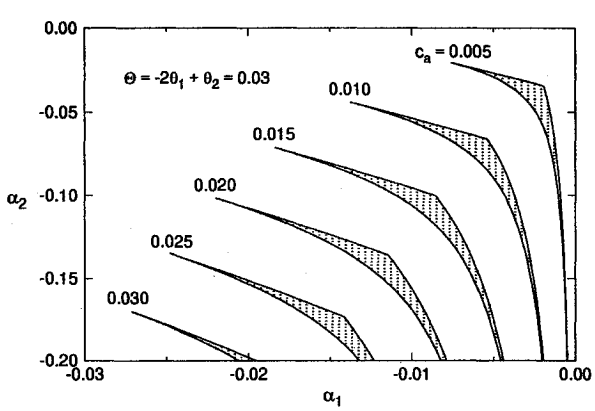

Fig. 1 Parameter region for existence of triggering to a stable limit cycle: case IIa, $\dot{m}_b' \propto |u'|$.

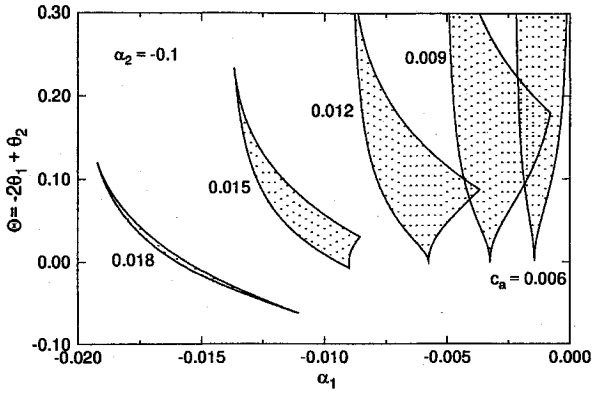

Fig. 2 Parameter region for existence of triggering to a stable limit cycle: case IIa, $\dot{m}_b' \propto |u'|$.

that energy transfer from higher modes to lower modes is very important in causing triggered instabilities. The current results show no required direction of the conservative energy flow between the modes caused from nonlinear gasdynamics. Although such transfer plays a key role in system behavior, triggering could occur with energy flow from the low to high mode or vice versa. However, the energy source term associated with nonlinear combustion in Eqs. (50) and (51) involves the product of both mode amplitudes, i.e., the presence of one mode is required to feed (or subtract) energy to (or from) the other. Physically, this might be interpreted as transfer of energy between modes, but it is not the usual transfer associated with nonlinear gasdynamics.

For case IIa, only two limit cycles may be found in a triggerable system, one stable and one unstable. A question central to the issue of triggered instability is, will a given initial condition (pulse) damp out or will it initiate instability (seek the stable limit cycle)? Yang et al.[1] showed that for a one-degree-of-freedom system (having third-order nonlinearity), triggering to a stable limit cycle could occur with an intermediate unstable limit cycle as the stability boundary. That is, pulses with initial energy larger than the unstable limit cycle would grow to the stable limit cycle, while smaller pulses would decay to zero. For the current multiple-degree-of-freedom scenario the stability boundary is represented by the unstable limit cycle between the stable limit cycle and trivial solution. More precisely, this is a hyperbolic equilibrium point whose stable manifold forms the stability boundary and whose invariant unstable manifold comprises a trajectory that typically attracts nearby solutions approaching the stable limit cycle or the stable trivial solution. For initial conditions close to the unstable manifold, the trajectory dynamics are similar to the one-dimensional model considered in Ref. 1, with the intermediate unstable limit cycle specifying the triggering threshold. Therefore, an approximate but somewhat naive determination of the region of stable initial pulses could be found by comparing initial energy of the system with the energy of the unstable limit cycle, i.e.,

$$\text{stable pulse if } \left[EM_i = \frac{E_1^2}{2\bar{\gamma}^2}\left(r_{1i}^2 + r_{2i}^2\right)\right] < \left[EM_u = \frac{E_1^2}{2\bar{\gamma}^2}\left(r_{1u}^2 + r_{2u}^2\right)\right] \tag{52}$$

where the subscripts i and u denote initial and unstable limit cycle values, respectively. This describes a circular sector on the r_1–r_2 plane, independent of Ψ_i, but is only valid for initial conditions near the manifold. For all other initial pulses, solution trajectories could be very different from the unstable manifold (especially initially). The difference in the energy flow between any particular trajectory and the unstable manifold's trajectory can be substantial, causing error in the approximate condition of Eq. (52). Unfortunately, no analytical expression was found to correct for the differences in energy flow. To find the region of stable pulses, the trajectory of each initial condition in a broad domain was numerically calculated for the example case IIa, whose parameters are given in Table 1. The parameters are chosen to most clearly portray representative triggering phenomena. Table 2 lists the location of the limit cycles in the example system. The solutions are calculated until the trivial solution or the stable limit cycle is reached. In some cases, the solution grew outside the range of validity of the second-order analysis, indicating incompleteness of the model for such pulses. For stable pulses, amplitude remained within limits and the model was adequate. Figure 3 shows the regions of stable pulses for system IIa with different initial phase differences between the two modes Ψ_i, including the approximate region from Eq. (52). With the exception of the $\Psi_i = 3\pi/2$ boundary, the approximate region is a reasonable, mostly conservative estimation of the actual nonlinear stability. For $\Psi_i = 3\pi/2$, the combustion response initially causes energy to rapidly flow out of the system, so by the time the solution nears the attracting trajectory, the initial composite amplitude has been effectively decreased. For $\Psi_i = \pi/2$, the initial effect of combustion response is most strongly driving, causing a shrunken stability boundary, but the effect is not as large as observed for $\Psi_i = 3\pi/2$. Also, there is a slight distortion of the stability region toward higher second mode amplitudes, suggesting that the amplitude of the second mode is not as important in determining stability behavior. In Refs. 10–12, experimental findings concluded that the spectral content, as

Table 1 Parameters for example systems

Parameter	Case IIa	Case IIb
α_1	−0.01	−0.0075
α_2	−0.093	−0.1
$\Theta = -2\theta_1 + \theta_2$	0.03	0.00
β	0.7164	0.7164
c_a, c_b	0.014	0.35

Table 2 Limit cycles for example cases

Type	r_{10}	r_{20}	Ψ_0
	Case IIa		
Stable	0.0912	0.0395	0.351π
Unstable	0.0348	0.0087	$0.358\pi/2$
	Case IIb		
Stable	0.0327	0.0168	0
Unstable	0.0143	0.0019	0

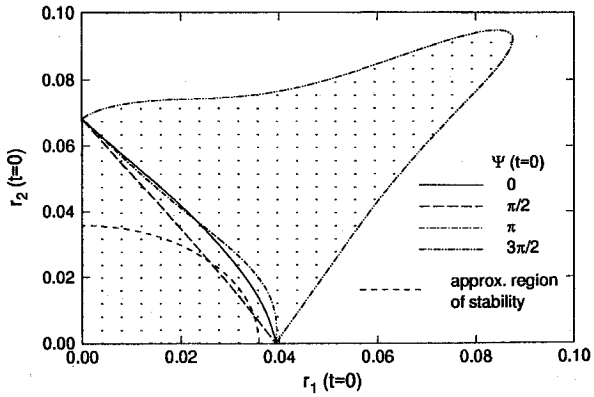

Fig. 3 Region of stable pulses for case IIa, $\dot{m}_b' \propto |u'|$.

well as the amplitude of the initial disturbance was important in determining stability. Specifically, triggering an instability was difficult if only the second mode was excited. This is consistent with the skewing of the stable region toward higher second-mode amplitudes.

The initial conditions for three different scenarios shown in Table 3 are chosen to explicitly demonstrate some of the important aspects of triggered instabilities, using the example case IIa in Table 2. Note that the initial composite amplitude ($r = \sqrt{r_{1i}^2 + r_{2i}^2}$) is the same for examples I and III, but smaller for example II. Figure 4 presents the time evolution of the mode amplitudes for examples I and II, showing the classic behavior which typifies triggered instabilities, small amplitude perturbations are damped out, while sufficiently large disturbances reach a finite limiting amplitude. There is also a period of relatively rapid change in mode amplitude immediately after the system is excited with the initial conditions. This initial period of adjustment has appeared in previous studies of nonlinear gasdynamics using time-averaging and a few-mode approximation, but has not been well addressed; as discussed previously, the energy gained or lost in this period can have important effects on the nonlinear stability of a system. To wit, Fig. 5 shows the mode amplitude evolution for examples I and III. Although the respective modes in each pulse have the same amplitude, the difference in initial phase difference initially causes energy to flow out of the system for example III, such that the pulse eventually decays. This is an example of the importance of initial phase on the stability of pulses.

Table 3 Initial conditions for example cases

Example	r_{1i}	r_{2i}	Ψ_i
	Case IIa		
I	0.03	0.05	0.0
II	0.03	0.01	0.0
III	0.03	0.05	$3\pi/2$
	Case IIb		
I	0.015	0.050	0.0
II	0.020	0.020	0.0
III	0.015	0.050	π

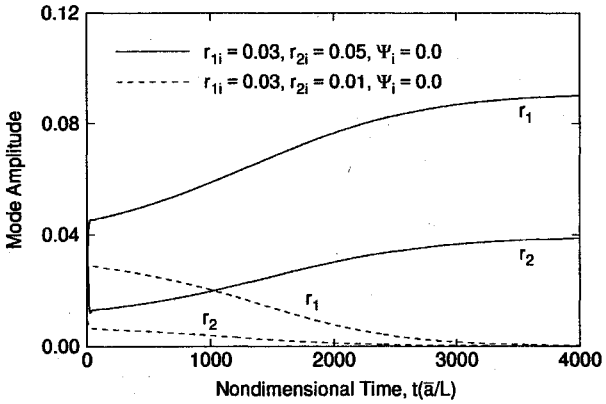

Fig. 4 Time evolution of mode amplitudes showing effect of initial mode amplitude on triggering, case IIa, $\dot{m}_b' \propto |u'|$.

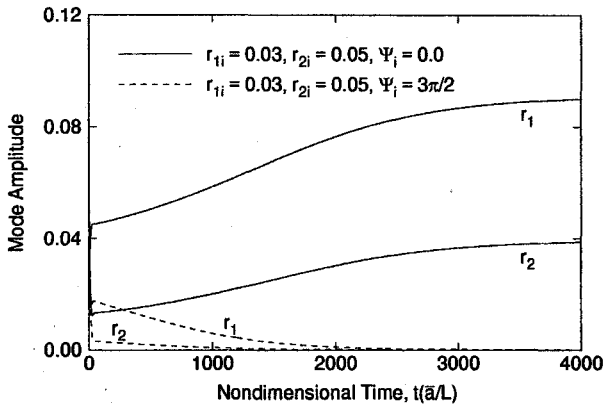

Fig. 5 Time evolution of mode amplitudes showing effect of initial phase on triggering, case IIa, $\dot{m}_b' \propto |u'|$.

C. Case IIb, $\dot{m}_b'$ Proportional to $p'|u'|$

For the case with $\dot{m}_b' \propto p'|u'|$, the following equations govern the changes in amplitude and phase difference:

$$\frac{dr_1}{dt} = \alpha_1 r_1 - \beta r_1 r_2 \cos\Psi - \frac{32c_b}{9} r_1^2 \cos\omega_1\tau_1 - \frac{64c_b}{45} r_2^2 \left\{\frac{3}{5}\cos[2\Psi + \omega_1(-5\tau_1 + 4\tau_2)] - \cos[2\Psi + \omega_1(-3\tau_1 + 4\tau_2)]\right\} \tag{53}$$

$$\frac{dr_2}{dt} = \alpha_2 r_2 + \beta r_1^2 \cos\Psi - \frac{32c_b r_1 r_2}{15} \times \left[\frac{7}{15}\cos[2\Psi + \omega_1(-4\tau_1 + 2\tau_2)] + 4\cos 2\omega_1\tau_2\right] \tag{54}$$

$$\frac{d\Psi}{dt} = \Theta + \left(2r_2 - \frac{r_1^2}{r_2}\right)\beta \sin\Psi + \frac{32c_b}{15}\left(\frac{4r_2^2}{3r_1}\left\{\frac{3}{5}\sin[2\Psi + \omega_2(-5\tau_1 + 4\tau_2)] + \sin[2\Psi + \omega_1(-3\tau_1 + 4\tau_2)]\right\} + r_1\left\{\frac{7}{15}\sin[2\Psi + \omega_1(-4\tau_1 + 2\tau_2)] - 4\sin 2\omega_1\tau_2 + 2\sin\omega_1\tau_1\right\}\right) \tag{55}$$

where

$$c_b = C_b\bar{a}^2 L/(\bar{\gamma}R_c\pi^2) \tag{56}$$

The equilibrium points (limit cycles) include the trivial solution and several finite limit cycles that are very complicated expressions in terms of the system parameters. The requirements for triggering are the same as for case IIa, but now a stable trivial solution demands only

$$\alpha_1 < 0, \qquad \alpha_2 < 0 \tag{57}$$

The complete region of triggering in the α_1–α_2 plane for $\Theta = 0$ is given in Fig. 6. For weak combustion response, very light damping of the first mode is required for triggering, although nearly any value of α_2 is allowed. For intermediate values of combustion response a broader region of triggering is found, with the ratio (α_2/α_1) restricted to a certain range. As combustion response increases, the region narrows (eventually disappearing), while favoring stronger first-mode damping. Figure 7 gives the triggering region for fixed $\alpha_2 = -0.1$ in terms of α_1 and Θ, yielding symmetric conditions for positive or negative phase difference parameters. For small combustion response, weakly damped first modes are required for triggering; as combustion response increases, the allowed range of Θ decreases, while the range of possible α_1 shifts toward stronger

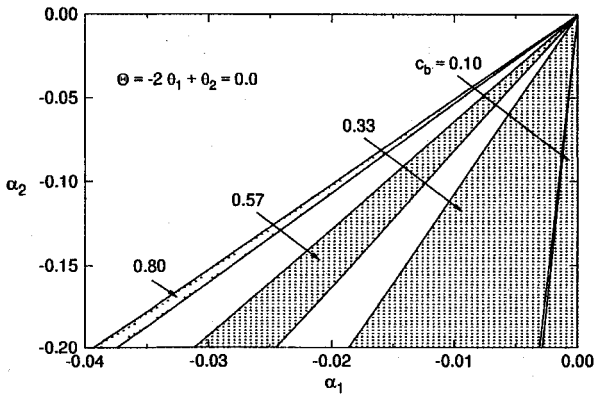

Fig. 6 Parameter region for existence of triggering to a stable limit cycle: case IIb, $\dot{m}_b' \propto p'|u'|$.

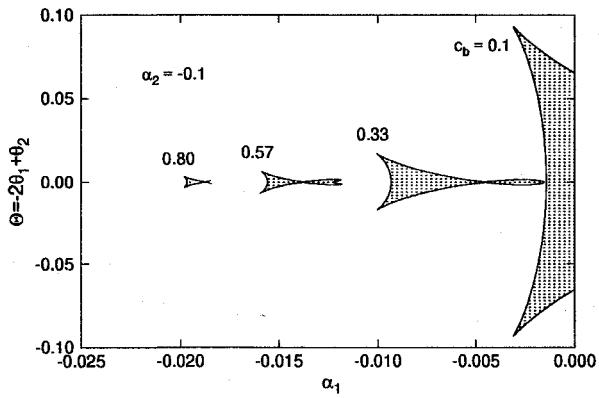

Fig. 7 Parameter region for existence of triggering to a stable limit cycle: case IIb, $\dot{m}_b' \propto p'|u'|$.

first-mode damping. These trends were also observed for case IIa. Note that for even moderate values of combustion response, relatively small deviation from $\Theta = 0$ may suppress triggered behavior.

For case IIb, the rates of change of energy for each mode are found to be

$$\frac{dEM_1}{dt} = \frac{E_1^2}{\bar{\gamma}^2}\left[\alpha_1 r_1^2 - \beta r_1^2 r_2 \cos\Psi - c_b\frac{16}{9}\left(r_1^3 - \frac{4}{25}\cos 2\Psi r_1 r_2^2\right)\right] \tag{58}$$

$$\frac{dEM_2}{dt} = \frac{E_2^2}{\bar{\gamma}^2}\left[\alpha_2 r_2^2 + \beta r_1^2 r_2 \cos\Psi - c_b\frac{16}{15}\left(4 + \frac{7}{15}\cos 2\Psi\right) r_1 r_2^2\right] \tag{59}$$

Here the effect of combustion is almost independent of mode phase if the second mode is sufficiently smaller than the first. For $\tau_1 = \tau_2 = 0$, the nonlinear combustion response can only drive the second mode [the last term in Eq. (59) is positive], but can damp the first depending on the relative magnitudes of the mode amplitudes and on Ψ [the last term in Eq. (58) can be positive or negative]. Also, no required direction was found for the conservative energy flow through nonlinear gasdynamics. As with case IIa, however, the nonlinear combustion response terms containing the product of mode amplitudes in Eqs. (58) and (59) might be confused as intermode energy transfer. The first mode has the additional r_1^3 term; unlike case IIa, the first mode can receive energy from nonlinear combustion independent of the second mode.

The example system used to study triggering for case IIb is given in Table 1, with the stable and unstable limit cycles listed in Table 2; there also existed four other unstable limit cycles, which are not listed since they did not appear to be important for causing triggering, although they did impact the nonlinear behavior. If $\Theta = 0$ in Eq. (55) and the initial pulse has $\Psi_i = 0$, with the combustion response time lag set to zero ($\tau_1 = \tau_2 = 0$), then $\dot{\Psi} = 0$, and solutions for case IIb should lie in the $\Psi = 0$ plane. Figure 8 illustrates this situation, displaying the two-dimensional state space (r_1 and r_2). Equations (53) and (54) represent a vector field, the streamlines of which are solutions with time as a parameter along the trajectory. Three sample trajectories are shown with time markers (dots) on the trajectory at every 10 nondimensional time units. Considering trajectory A, initially, r_1 is much larger than r_2, and so there is relatively little damping because of the small magnitude of α_1. Energy transfer then occurs from the first to second mode through nonlinear gasdynamics. If no damping or driving were present, this energy transfer would move the solution upward along a circular arc centered at the origin, corresponding to a constant energy trajectory [with total $EM \propto (r_{1A}^2 + r_{2A}^2)/2$]. However, the driving effect of nonlinear combustion adds energy to both modes. At first, mode 1 receives more energy because of the initially small r_2, which is not easily transferred to mode 2 initially because of small r_2. Thus, the first part of trajectory A shows rapid growth in the first mode and slower growth in the second. As the second mode increases, its growth is accelerated by the proportionately increasing energy transfer from the first mode and energy extraction from combustion directly. Opposing these increases is the second-mode damping that eventually causes r_2 to decrease. Mode 1 amplitude had already begun decreasing because of the enhanced transfer of energy to the growing second mode, and to a lesser extent because of the reduction in combustion driving caused by the r_2^2 term in Eq. (58). With the first mode decreasing, the second mode will also decrease because the r_1-dependent driving of mode 2 (energy transfer from mode 1 and combustion response) lessens, while the strong second-mode damping dominates. The second mode therefore decreases quite rapidly until the trajectory approaches the attracting trajectory of the limit cycle. Up to this point in the solution, the dominant processes have been relatively fast-acting. Near the unstable manifold of the unstable limit cycle (the attracting trajectory), however, the system achieves a state in which the energy damping and driving processes (especially the linear damping of the second mode and the energy transfer to the second mode) are almost balanced. After this, any rapid changes in r_1 or r_2 would be resisted by these fairly fast-acting processes. As a result, the approach toward the stable limit cycle occurs more slowly than the initial transition from the initial condition to the unstable manifold trajectory. This is seen very clearly for trajectory C.

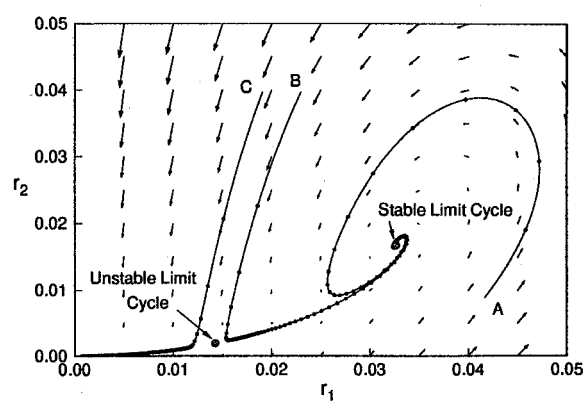

Fig. 8 State-space representation of triggered solutions on $\Psi = 0$ plane for case IIb, $\dot{m}_b' \propto p'|u'|$, $\Theta = 0$, and $\Psi_i = 0$.

Here the initial amplitude of the first mode is low enough so that the strong damping of the second mode dominates the behavior in the initial adjustment period. Once the solution approaches the attracting trajectory, slower behavior is observed as the solution damps away. Similar behavior is observed for trajectory B, but here the system maintains sufficient energy to attain the nonzero limit cycle.

Equation (52) is used to approximate the region of stable pulses for case IIb, which is shown in Fig. 9 along with the actual region obtained from numerical calculations of Eqs. (53–55). Substantial differences are observed between this plot and Fig. 3. First, whether a pulse is stable or not seems to depend primarily on the initial amplitude of the first mode, e.g., if r_1 is smaller than the amplitude of the unstable limit cycle, the pulse will likely damp out, even if r_2 (and hence the composite amplitude) are very large. As for case IIa, this shows agreement with the experimental findings in Refs. 10–12 that initiating instability through excitation of the second mode alone was difficult. The agreement is much stronger here than for case IIa, showing more influence of initial harmonic content on disturbance stability behavior. Second, the approximate region of stability is an extremely conservative estimate of the actual stability region for system IIb in the absolute sense. However, if stability is taken only as a function of first mode amplitude, then the unstable limit cycle amplitude appears to be a good estimate of the boundary between stable and unstable pulses, at least for initial phase difference near $n\pi/2$, n odd. Third, for $\Psi_i = 0$, the region of stable pulses completely encircles the stable limit cycle, indicating that very large pulses would be stable, regardless of harmonic content. Finally, for $\Psi_i = \pi$, an additional band of stable pulses is found. In this region, pulse stability is increased if the initial amplitude of the second mode is small, or if the amplitude of the first is decreased, but not made too small. Such complicated behavior is attributed to the additional unstable limit cycles, and serves to underscore the general finding that initial phase difference and harmonic content can be just as important as initial composite amplitude in determining the stability of a pulse.

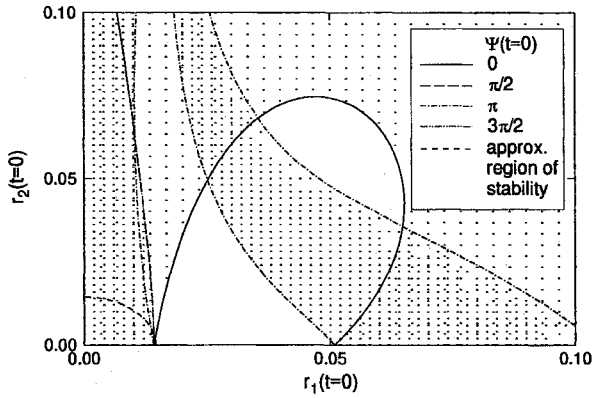

Fig. 9 Region of stable pulses for case IIb, $\dot{m}_b' \propto p'|u'|$.

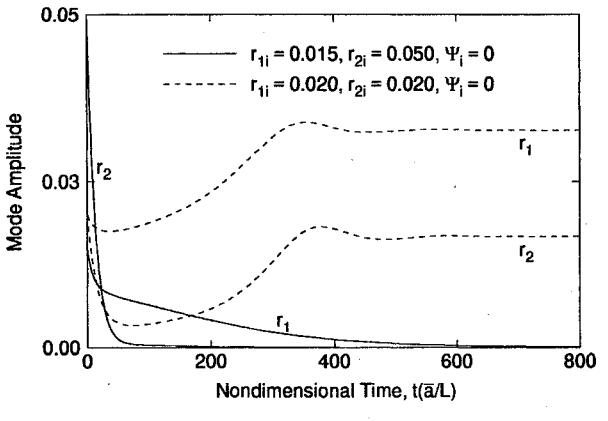

Fig. 10 Time evolution of mode amplitudes showing effect of initial mode amplitude on triggering, case IIb, $\dot{m}_b' \propto p'|u'|$.

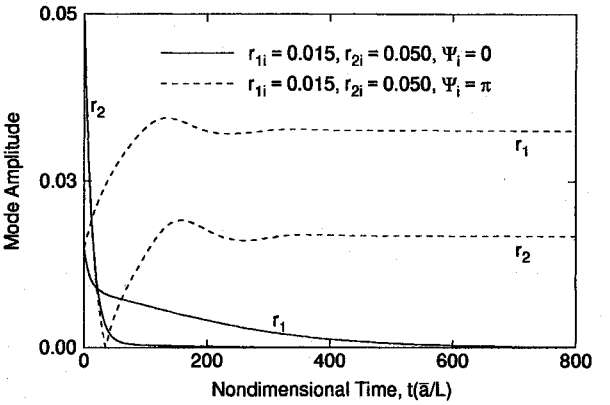

Fig. 11 Time evolution of mode amplitudes showing effect of initial phase on triggering, case IIb, $\dot{m}_b' \propto p'|u'|$.

Table 3 gives the initial conditions for three example pulses for case IIb. Figure 10 compares the mode amplitude histories for examples I and II, illustrating the importance of initial harmonic content on stability. Although the initial composite amplitude of the pulse for example I is about twice that of example II, it decays while the pulse for example II grows to the limit cycle. In Fig. 11, both pulses initially have identical mode amplitudes, but the difference in phase causes example III to grow to the limit cycle, while example I decays. Overall, the initial adjustment period appears to be longer for case IIb scenarios than in case IIa, while the time required for oscillations to damp or reach a limit cycle is generally shorter than in Figs. 4 and 5.

V. Conclusions

A model based on the two-phase formulation of Culick and Yang[15] has been used to investigate triggering in solid rocket motors, extending the work by Yang et al.[1] Nonlinear combustion was the primary mechanism that was studied as a cause of triggering. The following was found:

1) To second order in fluctuation amplitude, nonlinear combustion response proportional to quadratic functions of acoustic pressure and velocity (i.e., $\dot{m}_b' \propto u'$, p', u'^2, p'^2, and $u'p'$, etc.) was found incapable of triggering a finite initial disturbance to a stable limit cycle.

2) For combustion response functions dependent on rectified acoustic velocity (i.e., $\dot{m}_b' \propto |u'|$, and $p'|u'|$, etc.), triggering to a stable limit cycle was possible.

The creation of linear cross coupling among the acoustic modes, and quadratic self-coupling of the fundamental mode was how the two classes of nonlinear combustion response ($\dot{m}_b' \propto |u'|$ and $\dot{m}_b' \propto p'|u'|$, respectively) caused triggering. Both cases seemed to require strong damping of the higher mode and weak damping of the lower mode for triggering. Also, for higher values of combustion response, the damping of both higher and lower modes should increase to maintain triggering.

The typical structure of a triggerable system entails a stable trivial solution, a stable nonzero limit cycle, and an unstable limit cycle with intermediate amplitude. For $\dot{m}_b' \propto |u'|$, the unstable limit cycle amplitude gave a generally conservative approximation of the threshold amplitude, although the threshold amplitude varied significantly with initial mode phases and slightly with initial harmonic content. For $\dot{m}_b' \propto p'|u'|$, initial harmonic content was important in determining stability of a pulse; roughly, for a two-mode system, the initial amplitude of the first mode had to be larger than the unstable limit cycle for the pulse to trigger, regardless of the second-mode ampli-

tude. Also for this case, initial phase can substantially broaden the stable region of pulses. In general, the initial harmonic content and phase relationship of a disturbance, as well as initial composite amplitude, should be considered with respect to triggered instabilities. The waveform (e.g., traveling wave, standing wave, bomb pulse, and harmonic disturbance, etc.) plays an important role in determining the dynamic behavior of the system.

References

[1]Yang, V., Kim, S. I., and Culick, F. E. C., "Triggering of Longitudinal Pressure Oscillations in Combustion Chambers, Part I: Nonlinear Gasdynamics," *Combustion Science and Technology*, Vol. 72, Nos. 4–6, 1990, pp. 183–214.

[2]Greene, W. D., "Triggering of Longitudinal Combustion Instabilities in Rocket Motors," M.S. Thesis, Dept. of Aerospace Engineering, Pennsylvania State Univ., University Park, PA, Dec. 1990.

[3]Kim, S. I., "Nonlinear Pressure Oscillations in Combustion Chambers," Ph.D. Dissertation, Dept. of Mechanical Engineering, Pennsylvania State Univ., University Park, PA, May 1989.

[4]Sirignano, W. A., and Crocco, L., "A Shock Wave Model of Unstable Rocket Combustion," *AIAA Journal*, Vol. 2, No. 7, 1964, pp. 1285–1296.

[5]Crocco, L., and Mitchell, C. E., "Nonlinear Periodic Oscillations in Rocket Motors with Distributed Combustion," *Combustion Science and Technology*, Vol. 1, No. 1, 1969, pp. 147–169.

[6]Levine, J. N., and Baum, J. D., "Numerical Techniques for Solving Nonlinear Instability Problems in Solid Rocket Motors," *AIAA Journal*, Vol. 20, No. 7, 1982, pp. 955–961.

[7]Levine, J. N., and Baum, J. D., "Modeling of Nonlinear Combustion Instability in Solid Propellant Rocket Motors," *Proceedings of the 19th Symposium (International) on Combustion*, The Combustion Inst., Pittsburgh, PA, 1982, pp. 769–776.

[8]Baum, J. D., Levine, J. N., and Lovine, R. L., "Pulse-Triggered Nonlinear Combustion Instability in Solid Rocket Motors," *AIAA Journal*, Vol. 22, No. 10, 1984, pp. 1413–1419.

[9]Baum, J. D., Levine, J. N., and Lovine, R. L., "Pulsed Instability in Rocket Motors: A Comparison Between Predictions and Experiment," *Journal of Propulsion and Power*, Vol. 4, No. 4, 1988, pp. 308–316.

[10]Lovine, R. L., and Micheli, P. L., "Nonlinear Stability for Tactical Motors. Volume I—Program Summary," Air Force Rocket Propulsion Lab., TR-85-017, Oct. 1985.

[11]Micheli, P. L., "Nonlinear Stability for Tactical Motors. Volume II—Mechanism Study," Air Force Rocket Propulsion Lab., TR-85-017, Feb. 1986.

[12]Micheli, P. L., and Flandro, G. A., "Nonlinear Stability for Tactical Motors. Volume III—Analysis of Nonlinear Solid Propellant Combustion Instability," Air Force Rocket Propulsion Lab., TR-85-017, Feb. 1986.

[13]Blomshield, F. S., Jolley, W. H., Harris, P. G., and Tandy, I. F. S., "Program Overview. Joint Report Volume 1," Technical Panel W-4: Propulsion Technology, KTA-11: Pulsed Nonlinear Combustion Instability, The Technical Cooperation Program, Oct. 1991.

[14]Levine, J. N., and Lovine, R. L., "Nonlinear Analysis of Motor Firing Data. Phillips Laboratory Report Volume V: Part B," Technical Panel W-4: Propulsion Technology, KTA-11: Pulsed Nonlinear Combustion Instability, The Technical Cooperation Program, Oct. 1991.

[15]Culick, F. E. C., and Yang, V., "Prediction of the Stability of Unsteady Motions in Solid Propellants Rockets Motors," *Nonsteady Burning and Combustion Stability of Solid Propellants*, edited by L. DeLuca, E. W. Price, and M. Summerfield, Vol. 143, Progress in Astronautics and Aeronautics, AIAA, Washington, DC, 1992, pp. 719–779.

[16]Culick, F. E. C., "Nonlinear Behavior of Acoustic Waves in Combustion Chambers," *Acta Astronautics*, Vol. 3, 1976, pp. 715–734.

[17]Yang, V., and Culick, F. E. C., "On the Existence and Stability of Limit Cycles for Transverse Acoustic Oscillations in a Cylindrical Combustion Chamber. 1: Standing Modes," *Combustion Science and Technology*, Vol. 72, Nos. 1–3, 1990, pp. 37–65.

[18]Rho, T. S., Tseng, I. S., and Yang, V., "Effects of Acoustic Oscillations on Flame Dynamics of Homogeneous Propellants in Rocket Motors," *Journal of Propulsion and Power*, Vol. 11, No. 4, 1995, pp. 640–650.

[19]Chu, W. W., Tseng, C. F., and Yang, V., "Interactions of Acoustic Waves and Premixed Flames in Porous Chambers, I: Numerical Simulation," *Combustion and Flame* (submitted for publication).

[20]Chu, W. W., Tseng, C. F., and Yang, V., "Interactions of Acoustic Waves and Premixed Flames in Porous Chambers, II: Theoretical Analysis," *Combustion and Flame* (submitted for publication).

[21]Crump, J. E., and Price, E. W., "Effect of Acoustic Environment on the Burning Rate of Solid Propellants," *AIAA Journal*, Vol. 2, No. 7, 1964, pp. 1274–1278.

[22]Jahnke, C. C., and Culick, F. E. C., "An Application of Dynamical Systems Theory to Nonlinear Combustion Instabilities," *Journal of Propulsion and Power*, Vol. 10, No. 4, 1994, pp. 508–517.